Inorganic Chemistry
Article

*Inorg. Chem.* **2009**, *48*, 6517–6525 **6517**
DOI: 10.1021/ic900425r

# Synthesis, Structure, and Luminescent Properties of Hybrid Inorganic−Organic Framework Materials Formed by Lead Aromatic Carboxylates: Inorganic Connectivity Variation from 0D to 3D

**Lei Zhang,[†,‡] Zhao-Ji Li,[†] Qi-Pu Lin,[†,‡] Ye-Yan Qin,[†] Jian Zhang,[†] Pei-Xiu Yin,[†,‡] Jian-Kai Cheng,[†] and Yuan-Gen Yao*[,†]**

[†]*The State Key Laboratory of Structural Chemistry, Fujian Institute of Research on the Structure of Matter, The Chinese Academy of Sciences, Fuzhou, Fujian 350002, P. R. China, and* [‡]*Graduate School of the Chinese Academy of Sciences, Bejing 100039, P. R. China*

Received March 3, 2009

The hydro(solvo)thermal reactions of $Pb(OAc)_2 \cdot 3H_2O$ with the aromatic carboxylic ligands 1,3,5-benzenetricarboxylic and 1,4-, 1,2-, and 1,3-benzenedicarboxylic acids (1,3,5-$H_3$BTC; 1,4-, 1,2-, and 1,3-$H_2$BDC) have yielded a family of inorganic−organic framework materials: $[Pb_2(1,3,5\text{-BTC})(\mu_3\text{-OH})(H_2O)]_n$ (**I**), $[NaPb(1,3,5\text{-BTC})(H_2O)]_n$ (**II**), $[Pb(1,4\text{-BDC})]_n$ (**III**), $[Pb_5(1,2\text{-BDC})_4(OAc)_2]_n$ (**IV**), and $\{[Pb_5(1,3\text{-BDC})_5(H_2O)_2]_2 \cdot H_2O\}_n$ (**V**). These complexes have been characterized by means of single-crystal X-ray diffraction, X-ray powder diffraction, thermogravimetric analysis−mass spectrometry, and photoluminescence spectra. They are all three-dimensional structures except for two-dimensional **IV**. Topology analysis reveals that complexes **I** an **V** represent rare (4,8)-connected flu and (3,4)-connected zeolite-like nets, respectively. The five complexes exhibit diverse inorganic connectivity, including a 0D $Pb_4O_{16}$ cluster for **I**, a 1D Pb−O−Pb chain for **II**, a 2D Pb−O−Pb network for **III** and **IV**, and an unprecedented 3D Pb−O−Pb framework for **V**. And the diversity in inorganic arrays leads to differences in luminescent properties of these complexes.

## Introduction

The preparation and study of hybrid inorganic−organic framework materials is an active area, owing to their intriguing network structures, new topologies, and potential applications.[1] According to the recent classification scheme of Cheetham and Rao, such hybrids can be divided into two categories: metal−organic coordination polymers and extended inorganic hybrids.[2] Numberless coordination polymers constructed from isolated metal ions or clusters and bridging organic ligands have been reported.[3] In contrast, extended inorganic hybrids which contain extended arrays of inorganic connectivity, M−X−M (M = metal, X = O, Cl, N, and S), remain less exploited. In truth, such compounds not only open up a vast area of new structures but provide a basis for creating materials with special magnetic, electronic, and optical properties that are traditionally found in metal oxides.[4] Both of these two kinds of hybrid framework materials can be classified on the basis of the dimensionality (*n*,*m*) of the inorganic (I) and organic (O) connectivities, defining a symbol $I^nO^m$.[2,4b] Some extended inorganic hybrids have been prepared, most of which represent 1D and 2D inorganic connectivities, such as $I^1O^0$, $I^1O^1$, $I^1O^2$, $I^2O^0$, and $I^2O^1$.[5] However, despite impressive progress in this area, fabrication of compounds that contain

*To whom correspondence should be addressed. Tel.: +86-591-83711523. Fax: +86-591-83714946. E-mail: yyg@fjirsm.ac.cn.

(1) (a) Férey, G. *Chem. Soc. Rev.* **2008**, *37*, 191. (b) Hill, R. J.; Long, D. L.; Champness, N. R.; Hubberstey, P.; Schröder, M. *Acc. Chem. Res.* **2005**, *38*, 377. (c) Blake, A. J.; Champness, N. R.; Hubberstey, P.; Li, W. S.; Withersby, M. A.; Schröder, M. *Coord. Chem. Rev.* **1999**, *183*, 117. (d) Moulton, B.; Zaworotko, M. J. *Chem. Rev.* **2001**, *101*, 1629. (e) Humphrey, S. M.; Oungoulian, S. E.; Yoon, J. W.; Hwang, Y. K.; Wise, E. R.; Chang, J. S. *Chem. Commun.* **2008**, 2891. (f) Jain, P.; Dalal, N. S.; Toby, B. H.; Kroto, H. W.; Cheetham, A. K. *J. Am. Chem. Soc.* **2008**, *130*, 10450. (g) Merrill, C. A.; Cheetham, A. K. *Inorg. Chem.* **2007**, *46*, 278. (h) Bauer, S.; Serre, C.; Devic, T.; Horcajada, P.; Marrot, J.; Férey, G.; Stock, N. *Inorg. Chem.* **2008**, *47*, 7568.

(2) Cheetham, A. K.; Rao, C. N. R.; Feller, R. K. *Chem. Commun.* **2006**, 4780.

(3) (a) Eddaoudi, M.; Moler, D. B.; Li, H. L.; Chen, B. L.; Reineke, T. M.; O'Keeffe, M.; Yaghi, O. M. *Acc. Chem. Res.* **2001**, *34*, 319. (b) Yaghi, O. M.; O'Keeffe, M.; Ockwig, N. W.; Chae, H. K.; Eddaoudi, M.; Kim, J. *Nature* **2003**, *423*, 705. (c) Dinca, M.; Long, J. R. *Angew. Chem., Int. Ed.* **2008**, *47*, 6766. (d) Martin, D. P.; Montney, M. R.; Supkowski, R. M.; LaDuca, R. L. *Cryst. Growth Des.* **2008**, *8*, 3091. (e) Ouellette, W.; Wang, G.; Liu, H.; Yee, G. T.; O'Connor, C. J.; Zubieta, J. *Inorg. Chem.* **2009**, *48*, 953. (f) Zhang, L.; Zhang, J.; Li, Z. J.; Qin, Y. Y.; Lin, Q. P.; Yao, Y. G. *Chem.—Eur. J.* **2009**, *15*, 989.

(4) (a) Cheetham, A. K.; Rao, C. N. R. *Science* **2007**, *318*, 58. (b) Rao, C. N. R.; Cheetham, A. K.; Thirumurugan, A. *J. Phys.: Condens. Matter* **2008**, *20*, 083202.

(5) (a) Falcão, E. H. L.; Naraso; Feller, R. K.; Wu, G.; Wudl, F.; Cheetham, A. K. *Inorg. Chem.* **2008**, *47*, 8336. (b) Thirumurugan, A.; Sanguramath, R. A.; Rao, C. N. R. *Inorg. Chem.* **2008**, *47*, 823. (c) Miller, S. R.; Wright, P. A.; Serre, C.; Loiseau, T.; Marrot, J.; Férey, G. *Chem. Commun.* **2005**, 3850. (d) Zhang, L.; Li, Z. J.; Qin, Y. Y.; Zhang, J.; Cheng, J. K.; Yin, P. X.; Yao, Y. G. *CrystEngComm* **2008**, *10*, 655. (e) Rao, K. P.; Thirumurugan, A.; Rao, C. N. R. *Chem.—Eur. J.* **2007**, *13*, 3193. (f) Zhang, L.; Zhang, J.; Li, Z. J.; Cheng, J. K.; Yin, P. X.; Yao, Y. G. *Inorg. Chem.* **2007**, *46*, 5838. (g) Dan, M.; Cheetham, A. K.; Rao, C. N. R. *Inorg. Chem.* **2006**, *45*, 8227.

© 2009 American Chemical Society
Published on Web 06/15/2009

3D inorganic connectivity remains a challenge. To the best of our knowledge, only five examples have been reported ($I^3O^0$ and $I^3O^1$), one of which based on pyridine dicarboxylate and the other four based on aliphatic dicarboxylates.[6] As for the extremely familiar aromatic carboxylates, there is no such example, because the lack of ligand flexibility has been a disadvantage for forming extended 3D inorganic connectivity.[2]

A possible solution might be the introduction of metal atoms with a large radius to form an expanded inorganic framework, admitting rigid aromatic carboxylic ligands. As a heavy p-block metal ion, $Pb^{2+}$ has importance in electroluminescence, photovoltaic conversion, and fluorescent sensors.[7] And the large radius and flexible coordination environment of $Pb^{2+}$ also provide unique opportunities for the formation of extended inorganic hybrids. If condensed Pb−O−Pb connectivity could be adopted by hybrid materials, the above valuable physical properties might be perfectly reserved, especially when the organic block consists of conjugated aromatic ligands. Although several Pb−aromatic carboxylates have been reported, their inorganic connectivities are mostly 0D clusters and 1D chains.[8]

Herein, we report a comprehensive study of a Pb−aromatic carboxylate hybrid family with interesting inorganic connectivity diversity: a 0D $Pb_4O_{16}$ cluster for $[Pb_2(1,3,5\text{-BTC})(\mu_3\text{-OH})(H_2O)]_n$ (**I**), a 1D Pb−O−Pb chain for $[NaPb(1,3,5\text{-BTC})(H_2O)]_n$ (**II**), a 2D Pb−O−Pb layer for $[Pb(1,4\text{-BDC})]_n$ (**III**), a 2D Pb−O−Pb layer for $[Pb_5(1,2\text{-BDC})_4(OAc)_2]_n$ (**IV**), and a 3D Pb−O−Pb framework for $\{[Pb_5(1,3\text{-BDC})_5(H_2O)_2]_2\cdot H_2O\}_n$ (**V**). The unprecedented 3D inorganic connectivity in **V** is first found in aromatic carboxylates, making a great breakthrough in the area of extended inorganic hybrids. The structures and physical properties of these five compounds are described and discussed. In particular, the inorganic arrays indicate intense influences on their photoluminescence properties.

## Experimental Section

**Materials and Instrumentation.** Commercially available reagents were used as received without further purification. All syntheses were carried out in 23 mL poly(tetrafluoroethylene)-lined stainless steel containers under autogenous pressure. The elemental analyses were performed on an EA1110 CHNS-0 CE elemental analyzer. The IR spectroscopy was recorded on a PECO (U.S.A.) SpectrumOne spectrophotometer with pressed KBr pellets. The thermal decomposition behavior was analyzed by thermogravimetric analysis−mass spectrometry analysis (TGA-MS) using the NETSCH STA-449C thermoanalyzer coupled with a NETSCH QMS403C mass spectrometer. The fluorescence measurements were performed on polycrystalline or powder samples at room temperature using an Edinburgh FLS920 TCSPC fluorescence spectrophotometer. The phase purity and crystallinity of each product were checked by powder X-ray diffraction (XRD) using a Rigaku Dmax2500 diffractometer with Cu Kα radiation ($\lambda$ = 1.54056 Å). A step size of 0.05° and a counting time of 1.2 s/step were applied in a 2$\theta$ range of 5.00−55.00°.

**Synthesis of $[Pb_2(1,3,5\text{-BTC})(\mu_3\text{-OH})(H_2O)]_n$ (I).** A mixture of 1,3,5-$H_3$BTC (0.211 g, 1.0 mmol), melamine (0.066 g, 0.5 mmol), and $Pb(OAc)_2\cdot 3H_2O$ (0.761 g, 2.0 mmol) was placed in a 23 mL Teflon liner; 5 mL of ethanol and 10 mL of water were then added. The resulting mixture was sealed in a Parr autoclave. The autoclave was then placed in a programmable furnace and heated to 170 °C. The temperature was held for 3 days, and then the reactant mixture was cooled at a rate of 0.5 °C $min^{-1}$ to form colorless block crystals of **I**. Yield: 60%. Anal. calcd (%) for $C_9H_6Pb_2O_8$: C, 16.47; H, 0.92. Found: C, 16.41; H, 1.01%. IR (solid KBr pellet, v/$cm^{-1}$) for complex **I**: 3185 (m), 1605 (m), 1539 (s), 1427 (s), 1366 (s), 1103 (w), 931 (w), 765 (w), 721 (m), 508 (w).

**Synthesis of $[NaPb(1,3,5\text{-BTC})(H_2O)]_n$ (II).** The reaction was carried out in a procedure similar to that for **I**, only increasing the amount of melamine to 0.125 g (1.0 mmol) and adding NaOH (0.042 g, 1.0 mmol). Colorless sheet crystals of **II** were isolated in 55% yield. Anal. calcd (%) for $C_{18}H_{10}Na_2Pb_2O_{14}$: C, 23.74; H, 1.11. Found: C, 23.83; H, 1.04%. IR (solid KBr pellet, v/$cm^{-1}$) for complex **II**: 3013 (m), 1615 (m), 1544 (m), 1427 (s), 1357 (s), 1103 (w), 819 (w), 763 (w), 721 (m), 516 (w).

**Synthesis of $[Pb(1,4\text{-BDC})]_n$ (III).** A mixture of 1,4-$H_2$BDC (0.166 g, 1.0 mmol), melamine (0.063 g, 0.5 mmol), and $Pb(OAc)_2\cdot 3H_2O$ (0.381 g, 1.0 mmol) was placed in a 23 mL Teflon liner; 5 mL of ethanol and 10 mL of water were then added. The resulting mixture was sealed in a Parr autoclave. The autoclave was then placed in a programmable furnace and heated to 170 °C. The temperature was held for 3 days, and then the reactant mixture was cooled at a rate of 0.5 °C $min^{-1}$ to form colorless prism crystals of **III**. Yield: 65%. Anal. calcd (%) for $C_8H_4PbO_4$: C, 25.88; H, 1.09. Found: C, 25.96; H, 1.01%. IR (solid KBr pellet, v/$cm^{-1}$) for complex **III**: 3401 (w), 2919 (w), 1627 (w), 1402 (vs), 1050 (w), 838 (w), 818 (w), 750 (w), 677 (m), 514 (w).

**Synthesis of $[Pb_5(1,2\text{-BDC})_4(OAc)_2]_n$ (IV).** The reaction was carried out in a procedure similar to that for **III**, using 1,2-$H_2$BDC (0.167 g, 1.0 mmol) instead of 1,4-$H_2$BDC and increasing the amount of melamine to 0.127 g (1.0 mmol). Colorless sheet crystals of **IV** were isolated in 58% yield. Anal. calcd (%) for $C_{36}H_{22}Pb_5O_{20}$: C, 23.88; H, 1.22. Found: C, 23.95; H, 1.19%. IR (solid KBr pellet, v/$cm^{-1}$) for complex **IV**: 3349 (w), 3184 (w), 1639 (w), 1513 (s), 1485 (s), 1397 (m), 1378 (m), 1036 (m), 1022 (m), 746 (w), 685 (w).

**Synthesis of $\{[Pb_5(1,3\text{-BDC})_5(H_2O)_2]_2\cdot H_2O\}_n$ (V).** A mixture of 1,3-$H_2$BDC (0.168 g, 1.0 mmol), melamine (0.065 g, 0.5 mmol), and $Pb(OAc)_2\cdot 3H_2O$ (0.195 g, 0.5 mmol) was placed in a 23 mL Teflon linear; 15 mL of water was then added. The resulting mixture was sealed in a Parr autoclave. The autoclave was then placed in a programmable furnace and heated to 170 °C. The temperature was held for 3 days, and then the reactant mixture was cooled at a rate of 0.5 °C $min^{-1}$ to form colorless block crystals of **V**. Yield: 61%. Anal. calcd (%) for $C_{160}H_{80}Pb_{20}O_{90}$: C, 25.33; H, 1.06. Found: C, 25.42; H, 1.02%. IR (solid KBr pellet, v/$cm^{-1}$) for complex **V**: 3391 (w), 3139 (m),

(6) (a) Huang, Y. G.; Wu, B. L.; Yuan, D. Q.; Xu, Y. Q.; Jiang, F. L.; Hong, M. C. *Inorg. Chem.* **2007**, *46*, 1171. (b) Forster, P. M.; Cheetham, A. K. *Angew. Chem., Int. Ed.* **2002**, *41*, 457. (c) Guillou, N.; Livage, C.; Drillon, M.; Férey, G. *Angew. Chem., Int. Ed.* **2003**, *42*, 5314. (d) Vaidhyanathan, R.; Natarajan, S.; Rao, C. N. R. *Dalton Trans.* **2003**, 1459. (e) Zhang, J.; Chen, S. M.; Valle, H.; Wong, M.; Austria, C.; Cruz, M.; Bu, X. H. *J. Am. Chem. Soc.* **2007**, *129*, 14168.

(7) (a) Nikol, H.; Vogler, A. *J. Am. Chem. Soc.* **1991**, *113*, 8988. (b) Dutta, S. K.; Perkovic, M. W. *Inorg. Chem.* **2002**, *41*, 6938. (c) Tsuboi, T.; Sifsten, P. *Phys. Rev. B* **1991**, *43*, 1777. (d) Ballardini, R.; Varani, G.; Indelli, M. T.; Scandola, F. *Inorg. Chem.* **1986**, *25*, 3858. (e) Yang, J.; Li, G. D.; Cao, J. J.; Yue, Q.; Li, G. H.; Chen, J. S. *Chem.—Eur. J.* **2007**, *13*, 3248.

(8) (a) Yang, E. C.; Li, J.; Ding, B.; Liang, Q. Q.; Wang, X. G.; Zhao, X. J. *CrystEngComm* **2008**, *10*, 158. (b) Schuy, A.; Ruschewitz, U. *Z. Anorg. Allg. Chem.* **2005**, *631*, 659. (c) Foreman, M. R. S. J.; Gelbrich, T.; Hursthouse, M. B.; Plater, M. J. *Inorg. Chem. Commun.* **2000**, *3*, 234. (d) Shi, J.; Ye, J. W.; Song, T. Y.; Zhang, D. J.; Ma, K. R.; Ha, J.; Xu, J. N.; Zhang, P. *Inorg. Chem. Commun.* **2007**, *10*, 1534. (e) Zhang, L.; Qin, Y. Y.; Li, Z. J.; Lin, Q. P.; Cheng, J. K.; Zhang, J.; Yao, Y. G. *Inorg. Chem.* **2008**, *47*, 8286. (f) Dale, S. H.; Elsegood, M. R. J.; Kainth, S. *Acta Crystallogr.* **2004**, *C60*, m76. (g) Wu, R. F.; Zhang, T. L.; Qiao, X. J.; Yang, L.; Zhang, H. G.; Hu, X. C. *J. Coord. Chem.* **2008**, *61*, 1437. (h) Deng, H. J.; Li, X. H. *Acta Crystallogr.* **2006**, *E62*, m2467. (i) Li, X. J.; Cao, R.; Guo, Z. G.; Lü, J. *Chem. Commun.* **2006**, 1938. (j) Zhang, Z.; Zhou, Y. L.; He, H. Y. *Acta Crystallogr.* **2006**, *E62*, m2591. (k) Marandi, F.; Ghorbanloo, M.; Soudi, A. A. *J. Coord. Chem.* **2007**, *60*, 1557.

**Table 1.** Crystal Data and Structure Refinements for Compounds **I**−**V**

| param | **I** | **II** | **III** | **IV** | **V** |
|---|---|---|---|---|---|
| formula | $C_9H_6Pb_2O_8$ | $C_{18}H_{10}Na_2Pb_2O_{14}$ | $C_8H_4PbO_4$ | $C_{36}H_{22}Pb_5O_{20}$ | $C_{160}H_{80}Pb_{20}O_{90}$ |
| fw | 656.54 | 910.64 | 371.31 | 1810.54 | 7586.25 |
| temp (*K*) | 293(2) | 293(2) | 293(2) | 293(2) | 293(2) |
| cryst syst | triclinic | orthorhombic | orthorhombic | triclinic | orthorhombic |
| space group | $P\bar{1}$ | *Pnma* | *Pbca* | $P\bar{1}$ | *Pnma* |
| *A* (Å) | 7.607(4) | 6.418(2) | 7.726(3) | 7.146(3) | 27.2552(11) |
| *B* (Å) | 7.737(4) | 10.099(3) | 10.277(5) | 10.323(4) | 20.1771(7) |
| *C* (Å) | 10.789(5) | 17.553(5) | 18.324(9) | 14.009(6) | 15.3894(5) |
| α (Å) | 69.521(15) | 90 | 90 | 109.922(15) | 90 |
| *B* (Å) | 69.965(15) | 90 | 90 | 92.24(2) | 90 |
| Γ (Å) | 88.79(2) | 90 | 90 | 105.002(16) | 90 |
| *V* (Å$^3$) | 555.3(5) | 1137.7(6) | 1454.9(12) | 929.2(7) | 8463.1(5) |
| *Z* | 2 | 2 | 8 | 1 | 2 |
| $D_{calcd}$ (g cm$^{-3}$) | 3.926 | 2.658 | 3.390 | 3.236 | 2.977 |
| $\mu$ (mm$^{-1}$) | 30.312 | 14.890 | 23.162 | 22.662 | 19.917 |
| restraints | 50 | 3 | 0 | 0 | 132 |
| largest diff. peak/hole (e Å$^{-3}$) | 3.602, −4.642 | 0.891, −0.968 | 1.543, −2.187 | 3.624, −3.987 | 2.922, −2.995 |
| GOF | 0.991 | 1.023 | 1.048 | 0.951 | 1.027 |
| R1[a] ($I > 2\sigma(I)$) | 0.0432 | 0.0198 | 0.0375 | 0.0453 | 0.0533 |
| wR2[a] (all data) | 0.0980 | 0.0614 | 0.1004 | 0.1007 | 0.1358 |

[a] $R1 = \sum||F_o| - |F_c||/\sum|F_o|$; $wR2 = \{\sum[w(F_o^2 - F_c^2)^2]/\sum[w(F_o^2)^2]\}^{1/2}$; $w = 1/[\sigma^2(F_o^2) + (aP)^2 + bP]$, where $P = [\max(F_o^2,0) + 2F_c^2]/3$ for all data.

1625 (w), 1533 (s), 1444 (m), 1368 (s), 1085 (w), 924 (w), 740 (w), 702 (w), 528 (w).

**X-Ray Crystallography.** Suitable single crystals of **I**−**V** were carefully selected under an optical microscope and glued to thin glass fibers. Structural measurements were performed on a computer-controlled Rigaku SCXmini CCD Diffractometer with graphite-monochromated Mo Kα radiation ($\lambda_{MoK\alpha}$ = 0.71073 Å) at $T$ = 293.2 K. Absorption corrections were made using the SADABS program.[9] The structures were solved using the direct method and refined by full-matrix least-squares methods on $F^2$ using the SHELX-97 program package.[10] All non-hydrogen atoms except those needed for disorder modelling were refined anistropically, and hydrogen atoms attached to carbon atoms were fixed at their ideal positions. The water hydrogen atoms were located from difference maps and refined with isotropic temperature factors. Crystal data as well as details of data collection and refinement of **I**−**V** are summarized in Table 1. Selected bond lengths and angles are given in Table S1 (Supporting Information).

The topology analyses for compounds **I** and **V** were studied using TOPOs 4.0.[11]

## Result and Discussion

**0D $Pb_4O_{16}$ Cluster and Flu Topology in $[Pb_2(1,3,5\text{-BTC})(\mu_3\text{-OH})(H_2O)]_n$ (I).** X-ray crystallographic analysis reveals that compound **I** is a 3D coordination polymer which crystallizes in the space group $P\bar{1}$. There are two crystallographically independent $Pb^{2+}$ ions, Pb1 and Pb2; one 1,3,5-BTC anion; one hydroxyl anion; and one terminal water molecule in the asymmetric unit. As shown in Figures 1a and 2a, Pb1 is hemidirected and coordinated by six oxygen atoms, forming a $Pb1O_6$ polyhedron. Among the six oxygen atoms, two are from the two $\mu_3$ hydroxyl anions (O1W and O1Wa), two are from the same 1,3,5-BTC anion (O3b and O4b), and the last two are from another two different 1,3,5-BTC anions

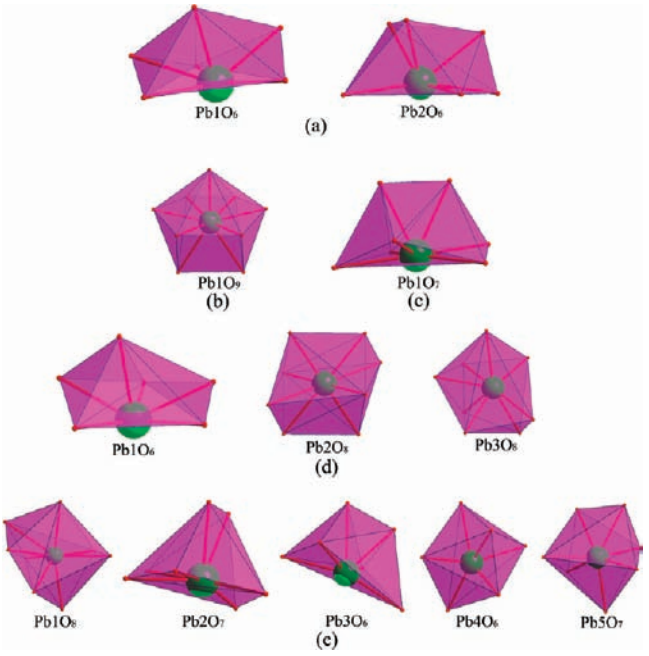


**Figure 1.** $PbO_n$ ($n$ = 6−9) polyhedra showing the coordination geometry of lead atoms in (a) **I**, (b) **II**, (c) **III**, (d) **IV**, and (e) **V**.

(O1 and O5c). The coordination environment of Pb2 is similar to that of Pb1, except a $\mu_3$ hydroxyl oxygen is replaced by a terminal water oxygen (O2W). The Pb−O bond lengths are in the 2.329−2.740 Å range. According to the research of Shimoni-Livny et al.,[12] the repulsion effect of the 6s lone pair electrons may result in long and weak coordination interactions around Pb. So, we have used bond order calculations to confirm the coordination environment of Pb centers. The analysis of bond valences reveals that the valences associated with the existing Pb−O bonds are 1.921 for Pb1 and 1.804 for Pb2. Although these values are less than the assumed oxidation state of Pb(II), there are no other weak Pb−O interactions.

(9) Sheldrick, G. M., *SADABS*; Institute for Inorganic Chemistry, University of Göttingen: Göttingen, Germany, 1996.
(10) Sheldrick, G. M., *SHELXL-97*; University of Göttingen: Göttingen, Germany, 1997.
(11) (a) Blatov, V. A.; Shevchenko, A. P.; Serezhkin, V. N. *Russ. J. Coord. Chem.* **1999**, *25*, 453. (b) Topos Main Page. http://www.topos.ssu.samara.ru (accessed June 2009).
(12) Shimoni-Livny, L.; Glusker, J. P.; Bock, C. W. *Inorg. Chem.* **1998**, *37*, 1853.

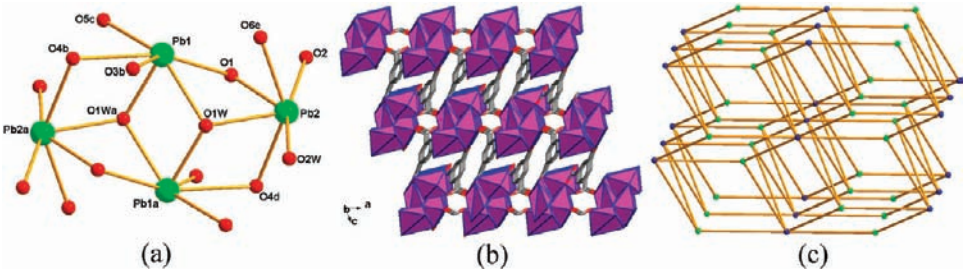


**Figure 2.** (a) Details of the coordination environments of Pb1 and Pb2 in complex **I** (symmetry codes: $a=1-x, 1-y, -z$; $b=-1+x, -1+y, 1+z$; $c=2-x, 2-y, -z$; $d=2-x, 2-y, -1-z$; $e=x, -1+y, z$). (b) A polyhedral representation of the 3D structure of **I**. (c) A schematic diagram of the flu topology of **I**.

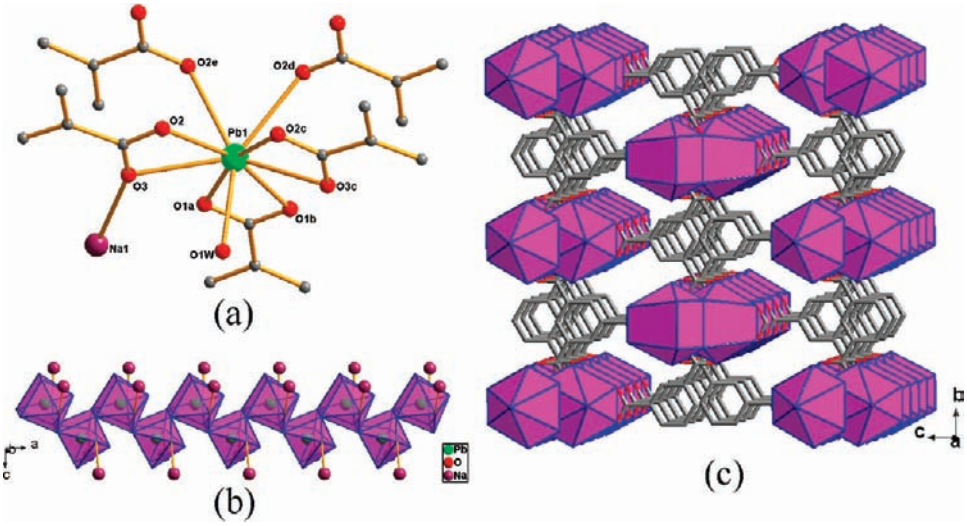


**Figure 3.** (a) The coordination environment of Pb1 in complex **II** (symmetry codes: $a=0.5-x, 1-y, 0.5+z$; $b=0.5-x, -0.5+y, 0.5+z$; $c=x, 0.5-y, z$; $d=-0.5+x, 0.5-y, 0.5-z$; $e=-0.5+x, y, 0.5-z$). (b) The 1D inorganic Pb−O−Pb chain in **II**. (c) A polyhedral representation of the 3D structure of **II**.

Whereas, in the other two reported Pb−benzenetricarboxylate complexes,[8c,8d] there are long Pb−O bonds up to 3.072 Å in length. The two $\mu_3$ hydroxyl anions bridge two Pb1 ions and two Pb2 ions into a planar $Pb_4$ cluster, with the two hydroxyls residing at the two sides of the plane (the distance from the hydroxyl to the plane is 0.7601 Å). The four $Pb1O_6$ and $Pb2O_6$ polyhedra form a unit of $Pb_4O_{16}$ by sharing an edge with an adjacent one. The carboxyl oxygens in the unit are from eight independent 1,3,5-BTC ligands. And every 1,3,5-BTC ligand is deprotonated and bridges six Pb ions from four different $Pb_4O_{16}$ units with a $\mu_6$-($\eta_2$-O,O′),($\eta_2$-O″,O‴),O′,O″,O⁗,O⁗′ coordination mode (Figure S1, Table 3). Finally, these connectivities between $Pb_4O_{16}$ units and ligands lead to the 3D framework of **I** with the $I^0O^3$ type (Figure 2b).

In the view of topology, the $Pb_4O_{16}$ unit and 1,3,5-BTC ligand are 8- and 4-connected nodes, respectively. Therefore, the whole structure can be defined as a bimodal (4,8)-connected net with long Schläfli symbols 4.4.4.4.4.4.4.4.4.4.4.$6^4$.$6^4$.$6^4$.$6^4$.$6^4$.$6^4$.$6^4$.$6^4$.$6^4$.$6^4$.$6^4$.$6^4$.$8^{24}$.$8^{24}$.$8^{24}$.$8^{24}$ and 4.4.4.4.4.4 for the two nodes (Figure 2c). And because the ratio of the unit to 1,3,5-BTC is 1:2, the short symbol becomes $(4^{12},6^{12},8^4)(4^6)_2$. Interestingly, this net has a strong balance to fluorite ($CaF_2$), one of the most important and preferred structures for $AB_2$-type compounds. To our knowledge, such a flu topology remains still rare in the area of inorganic−organic hybrids.[13]

**1D Pb−O−Pb Connectivity in [NaPb(1,3,5-BTC)($H_2O$)]$_n$ (II).** Complex **II** crystallizes in the space group *Pnma* and also is a 3D structure. Unlike **I**, it has a 1D extended inorganic connectivity of Pb−O−Pb. Each asymmetric unit contains one $Pb^{2+}$ ion, one $Na^+$ ion, one 1,3,5-BTC anion, and one coordinated water molecule. Pb1 is coordinated by nine oxygen atoms, with eight from five different 1,3,5-BTC ligands and the last one from terminal water, forming a holodirected geometry ($Pb1O_9$; Figures 1b and 3a). The Pb−O bond lengths are in the range of 2.546−2.786 Å. The valence calculated from the existing Pb−O bonds is 1.849 for Pb1. There are not any other weak Pb−O interactions. The Na ion is mono-coordinated by one carboxyl oxygen (Na1−O3, 2.766 Å). As shown in Figure 3b, these $Pb1O_9$ polyhedra share edges with each other, forming an infinite Pb−O−Pb chain, with Na ions decorating two sides. Among the three carboxyl groups of 1,3,5-BTC, one chelates to a Pb1 atom and the other two both bridge one Na atom and two Pb1 atoms in a $\mu_3$ fashion. Therefore, 1,3,5-BTC connects to two Na atoms and five Pb atoms with a $\mu_7$-($\eta_2$-O,O′),($\eta_2$-O″,O‴),($\eta_2$-O⁗,O⁗′),O″,O‴,O⁗,O⁗′ coordination mode (Figure S1, Supporting Information, Table 3), which has never been found before. These five Pb atoms

(13) (a) Chun, H.; Kim, D.; Dybtsev, D. N.; Kim, K. *Angew. Chem., Int. Ed.* **2004**, *43*, 971. (b) Li, S. L.; Lan, Y. Q.; Qin, J. S.; Ma, J. F.; Su, Z. M. *Cryst. Growth Des.* **2008**, *8*, 2055. (c) Zou, R. Q.; Zhong, R. Q.; Du, M.; Kiyobayashi, T.; Xu, Q. *Chem. Commun.* **2007**, 2467. (d) Taylor, K. M. L.; Athena, J.; Lin, W. *Angew. Chem., Int. Ed.* **2008**, *47*, 7722. (e) Wu, S.; Ma, L.; Long, L. S.; Zheng, L. S.; Lin, W. *Inorg. Chem.* **2009**, *48*, 2436.

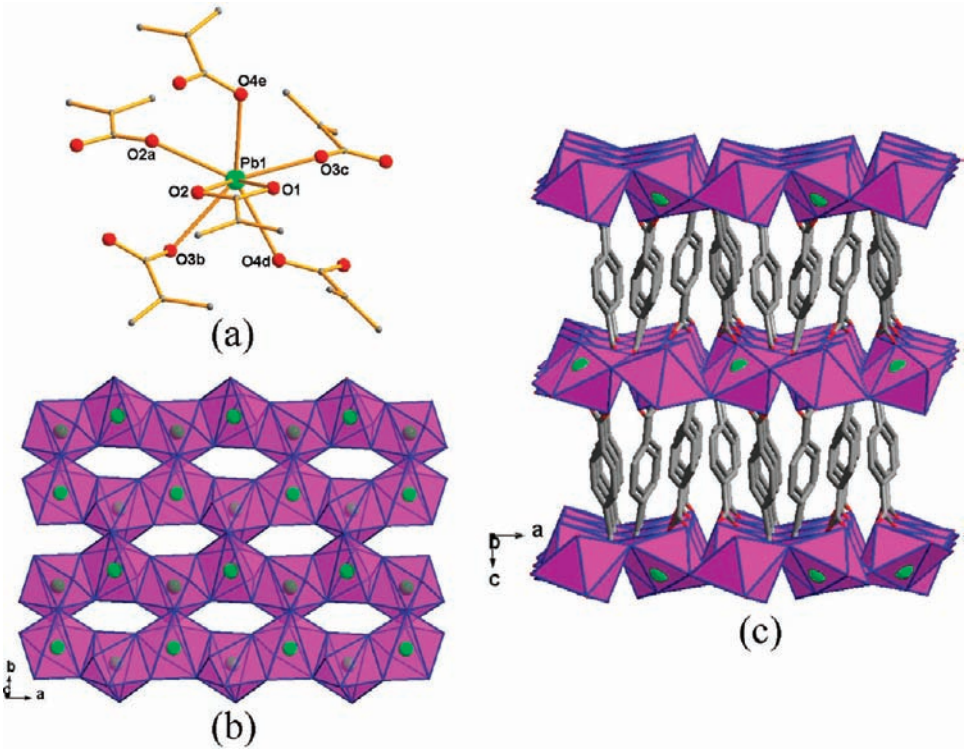


**Figure 4.** (a) The coordination geometry of Pb1 in complex **III** (symmetry codes: $a = 1-x,-1-y,-1-z$; $b = 0.5+x$, $y$, $-0.5-z$; $c = x$, $-0.5-y$, $-0.5+z$; $d = 1-x, 0.5+y, -0.5-z$; $e = 0.5-x, -1-y, -0.5+z$). (b) The 2D inorganic honeycomb Pb−O−Pb layer in **III**. (c) A polyhedral representation of the 3D structure of **III**.

are from three different Pb−O−Pb chains. Thus, each 1,3,5-BTC links three independent Pb−O−Pb chains together. And all of the 1D Pb−O−Pb chains are interconnected by the 1,3,5-BTC ligands to form the final 3D framework with the $I^1O^2$ type.

**2D Pb−O−Pb Connectivity in $[Pb(1,4\text{-BDC})]_n$ (III).** Complex **III** exhibits an interesting three-dimensional framework based on a 2D (6,3)-honeycomb inorganic Pb−O−Pb layer. There is only one crystallographically independent $Pb^{2+}$ ion, which is holodirected and coordinated by seven oxygen atoms from six different 1,4-BDC ligands (Figures 1c and 4a). The Pb−O bond lengths range from 2.498 to 2.785 Å, compared with 2.325 to 3.073 Å in the other 3D Pb−1,4-BDC structure, which is formed by 1,4-BDC ligands bridging 1D inorganic Pb−O−Pb chains.[8b] For complex **III**, there are no other weak Pb−O interactions, although the calculated valence is only 1.849 for Pb1. It should be pointed out that complex **III** has a very similar structure to the europium(II) terephthalate $[Eu(1,4\text{-BDC})]_n$ (**VI**) reported by Serre et al.,[14] which also represents 2D inorganic Eu−O−Eu layers. However, there are still some differences between the two structures owing to the different coordination geometries of $Pb^{2+}$ and $Eu^{2+}$ ions. Compared with seven-coordinated $Pb^{2+}$ in **III**, $Eu^{2+}$ in **VI** is bound to eight oxygen atoms from seven different 1,4-BDC's. Each 1,4-BDC ligand in **III** connects to six Pb1 atoms with a first found $\mu_6$-($\eta_2$-O,O′),O,O″,O‴,O⁗,O⁗⁗ mode, whereas each 1,4-BDC in **VI** links seven Eu1 atoms with a $\mu_7$-($\eta_2$-O,O′),O,O′,O″,O‴,O⁗,O⁗⁗ mode. As a result, these differences induce different built-up forms of the inorganic layers (Figure 4b): in **III**, each $Pb1O_7$ polyhedron shares three edges with three neighboring ones, while in **VI**, each $Eu1O_8$ polyhedron shares one edge and two faces with three adjacent ones. Finally, the inorganic Pb−O−Pb layers of **III** are combined together by 1,4-BDC ligands to give a 3D hybrid with the $I^2O^1$ type (Figure 4c).

**2D Pb−O−Pb Connectivity in $[Pb_5(1,2\text{-BDC})_4(OAc)_2]_n$ (IV).** Complex **IV** has a two-dimensional structure. Interestingly, it also contains a 2D inorganic Pb−O−Pb layer with 1,2-BDC and acetic ligands residing at the two sides, so it should be classified as the $I^2O^0$ type. The single-crystal X-ray structural analysis reveals that **IV** has three crystallographically independent $Pb^{2+}$ ions. As shown in Figures 1d and 5a, when only considering the relatively strong Pb−O bonds (Pb−O < 2.88 Å), Pb1 is coordinated by six oxygen atoms from five carboxyl groups of four different 1,2-BDC ligands, forming a hemidirected geometry. Pb2 is holodirected and bound to eight oxygen atoms from six different 1,2-BDC ligands. Pb3 is also holodirected and coordinated by eight oxygens, with one oxygen from an acetic ligand and the remaining seven oxygens from six carboxyl groups of five different 1,2-BDC ligands. And the Pb−O bond lengths are in the range of 2.501−2.793 Å. The valence associated with the existing Pb−O bonds is 1.653 for Pb1. Further calculation shows that two additional weak Pb−O interactions (Pb1−O7d, 2.889(7) Å; Pb1−O4b, 2.979(8) Å) also make considerable contributions, giving a new valence of 1.871. For Pb2, the valence associated with the existing Pb−O bonds is 1.545, and four additional weak Pb−O interactions (Pb2−O7d, 3.034(7) Å; Pb2−O7e, 3.034(7) Å; Pb2−O1, 3.039(7) Å; Pb2−O1c, 3.039(7) Å) increase the

(14) Serre, C.; Millange, F.; Marrot, J.; Férey, G. *Chem. Mater.* **2002**, *14*, 2409.

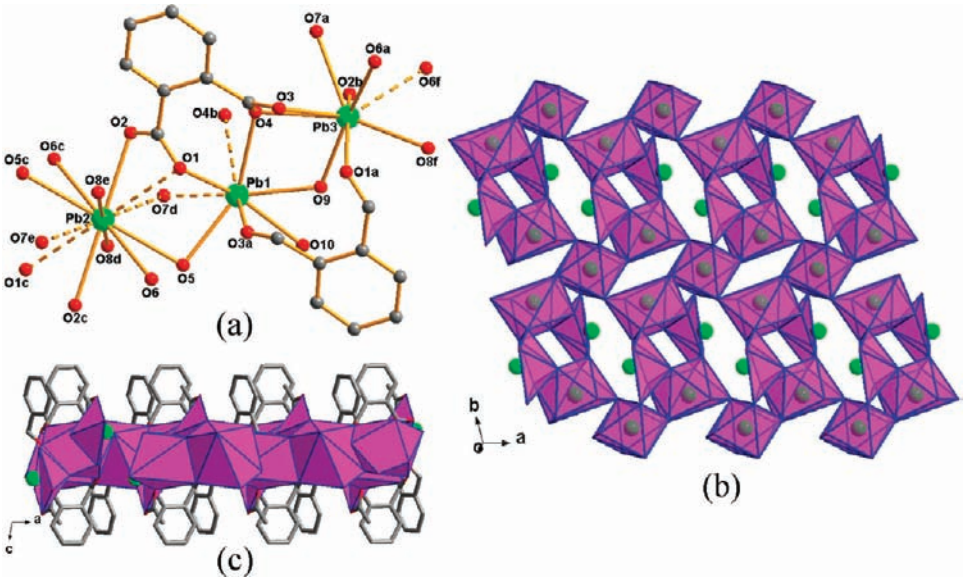


**Figure 5.** (a) The coordination environments of Pb1, Pb2, and Pb3 in complex **IV** (dashed bonds are weak Pb−O interactions found during bond order calculating; symmetry codes: $a=1-x,-y,1-z$; $b=2-x,-y,1-z$; $c=2-x,1-y,1-z$; $d=1+x,y,z$; $e=1-x,1-y,1-z$; $f=x,-1+y,z$). (b) The 2D inorganic Pb−O−Pb layer in **IV**. (c) A polyhedral representation of the 2D structure of **IV**.

valence to 1.874. For Pb3, one additional weak Pb−O interaction (Pb3−O6f, 2.918(7) Å) increases the valence from 1.808 to 1.921.

However, these weak Pb−O interactions do not change the inorganic connectivity of complex **IV**. And because of their long bond lengths and low bond energy, we omit these additional Pb−O interactions when discussing the accumulation of $PbO_n$ polyhedra and the luminescent properties of **III**. Each $Pb1O_6$ polyhedron shares one corner with one $Pb2O_8$ and two edges with two $Pb3O_8$'s. Each $Pb2O_8$ polyhedron shares two edges with two $Pb3O_8$'s and four corners with another two $Pb3O_8$'s and two $Pb1O_8$'s. Each $Pb3O_8$ polyhedron shares one corner with one $Pb2O_8$ and three edges with another $Pb2O_8$ and two $Pb1O_8$'s. Then, these connectivities link the polyhedra into the final 2D inorganic Pb−O−Pb layer (Figure 5b), which is decorated by 1,2-BDC and acetic ligands (Figure 5c). It is worth noting that there are three different kinds of rings in this layer, 3-, 4-, and 6-numbered, respectively. The 1,2-BDC ligands in **IV** can be divided into two types according to the coordination modes, $\mu_5$-($\eta_2$-O,O′),($\eta_2$-O′,O″),O,O‴,O‴ and $\mu_6$-($\eta_2$-O,O′),($\eta_2$-O′,O″),O′,O″,O‴,O‴ (Figure S1, Supporting Information, Table 3), both of which are reported for the first time.

**3D Pb−O−Pb Connectivity in $\{[Pb_5(1,3\text{-BDC})_5(H_2O)_2]_2\cdot H_2O\}_n$ (V).** Complex **V** is featured by its interesting 3D inorganic Pb−O−Pb framework, which is first found in aromatic carboxylates. There are five crystallographically independent $Pb^{2+}$ ions and eight 1,3-BDC ligands (two have full occupancy and six have half occupancy) in an asymmetric unit of **V**. Except two water oxygen atoms bonded to Pb3 and Pb5, all of the other coordinated oxygen atoms are from carboxylate groups. When only considering the relatively strong Pb−O bonds (Pb−O < 2.88 Å), the Pb−O bond lengths range from 2.257 to 2.870 Å, compared with 2.256 to 2.734 Å for another Pb−1,3-BDC complex.[8a] And O−Pb−O angles are between 47.280 and 174.622°. The valences associated with the existing Pb−O bonds are 1.830 for Pb1, 1.818 for Pb2, and 1.495 for Pb3. And further calculations show one additional weak Pb−O interaction (Pb1−O8, 3.044(10) Å) for Pb1, one additional weak Pb−O interaction (Pb2−O16c, 2.920(9) Å) for Pb2, and three additional weak Pb−O interactions (Pb3−O5, 2.926(8) Å; Pb3−O14, 2.990(8) Å; Pb3−O1, 3.030(10) Å) for Pb3, increasing their valences to 1.911, 1.951, and 1.783, respectively. For Pb4 and Pb5, the valences associated with the existing Pb−O bonds are 2.092 and 1.865, and there are not any other weak Pb−O interactions. These weak Pb−O interactions for Pb1, Pb2, and Pb3 do not change the inorganic connectivity of complex **V** and could be omitted during the next discussion. Therefore, Pb1 exhibits holodirected geometry with coordination number 8 (Figures 1e and 6a). Both Pb2 and Pb3 show hemidirected geometry with coordination numbers 7 and 6, respectively, whereas both 6-coordinated Pb4 and 7-coordinated Pb5 exhibit holodirected geometry. So, the Pb−O bonds for Pb1, Pb4, and Pb5 are more covalent than those for Pb2 and Pb3.[12,15] Each $Pb1O_8$ polyhedron shares one corner with one $Pb2O_7$ and three edges with $Pb4O_6$, $Pb5O_7$, and another $Pb2O_7$. Each $Pb2O_7$ polyhedron shares one edge with one $Pb1O_8$ and three corners with $Pb3O_6$, $Pb5O_7$, and another $Pb1O_8$. Each Pb3 is surrounded by another Pb3, Pb2, and Pb4, by sharing one edge and two corners of the $Pb3O_6$ polyhedron. The extending modes of the $Pb4O_6$ polyhedron and $Pb5O_7$ polyhedron are both like that of $Pb2O_7$, with Pb1, Pb3, Pb5, and another Pb4 around Pb4 and Pb1, Pb2, Pb4, and another Pb5 around Pb5. As shown in Figure 6b, the accumulating of these polyhedra gives the final 3D complicated oxide network. The most prominent feature of the inorganic skeleton is the presence of unidimensional pores running along the *a*, *b*, and *c* axes, with 10, 12, and 11 rings, respectively (Figures S2 and

(15) Watson, C. W.; Parker, S. C. *J. Phys. Chem. B* **1999**, *103*, 1258.

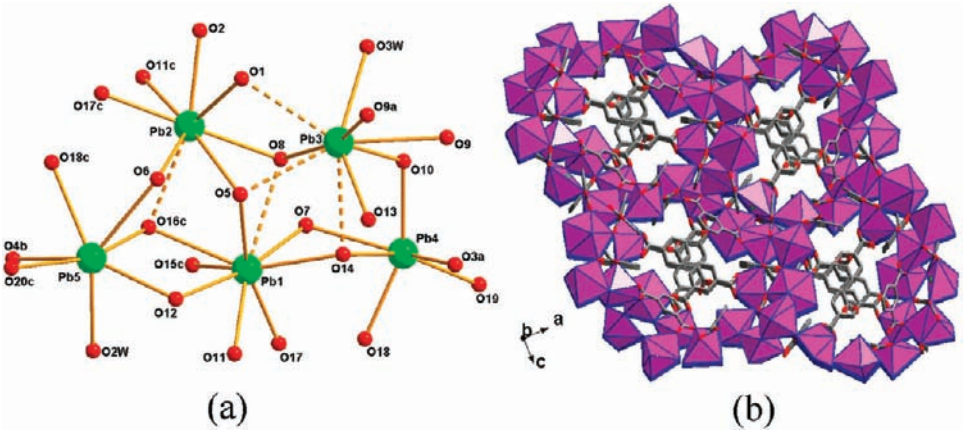


**Figure 6.** (a) Coordination environments of Pb(II) atoms in complex **V** (dashed bonds are weak Pb−O interactions found during bond order calculating; symmetry codes: $a = 1 - x, -y, 1 - z$; $b = -0.5 + x, y, 1.5 - z$; $c = 0.5 - x, -y, 0.5 + z$). (b) The 3D structure of **V** with polyhedral representation of the 3D inorganic Pb−O−Pb skeleton.

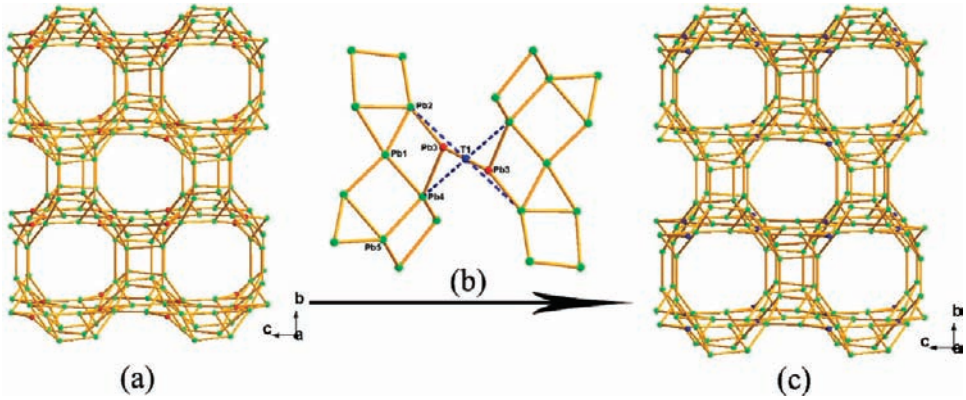


**Figure 7.** (a) Schematic representation of zeolite-like topology of the 3D inorganic skeleton of **V** (red and green represent 3- and 4- connected nodes, respectively). (b) The creation of a new 4- connected node (T1) by incorporating two adjacent 3- connected nodes. (c) The final zeolite net formed by nodes' incorporation (blue represents T1).

S3, Supporting Information). These pores are decorated by eight independent and deprotonated 1,3-BDC anions, with lattice water molecules residing in them. And according to the coordination modes, these ligands can be divided into five kinds, with one $\mu_3$-($\eta_2$-O,O′),O″,O‴, one $\mu_5$-($\eta_2$-O,O′),O,O″,O″,O‴, one $\mu_4$-O,O,O′,O′, two $\mu_8$-O,O,O′,O′,O″,O″,O‴,O‴, and three $\mu_6$-($\eta_2$-O,O′),($\eta_2$-O″,O‴),O,O′,O″,O‴ (Figure S1, Supporting Information, Table 3). Interestingly, in spite of the numberless 1,3-BDC complexes, the latter three coordination modes have never been reported before. And all of the bridging oxygen atoms are in the $\mu_2$ mode. It should be noted that when the Pb−O bonding limit extended to 3.07 Å, a pseudo-3D Pb−O−Pb framework was reported by Plater et al.[8c] However, such a long Pb−O bond is too weak to be considered as a significant action, and Rao et al. did not regard this compound as a hybrid with 3D inorganic connectivity.[2,4b] Therefore, **V** is strictly the first metal−aromatic carboxylate that represents 3D inorganic connectivity, with the unusual $I^3O^0$ type.

In order to understand the complicated inorganic skeleton more clearly, we use the topology analysis method to simplify this framework. On the basis of the above structure description, by treating Pb3 as a 3-connected node and Pb1, Pb2, Pb4, and Pb5 as 4-connected nodes and connecting the nodes according to the connectivity defined by the $\mu_2$-O atoms, the framework can be attached to a 5-nodal (3,4)-connected topology (Figure 7a). The long Schläfli symbol is 3.4.4.7.5.6 for Pb1, 4.4.4.8.6.6 for Pb2, 4.10.10 for Pb3, 3.7.4.4.5.5 for Pb4, and 3.4.4.7.5.6 for Pb5 (Table 2). So the short symbol for this 5-nodal net becomes $(3.4^2.5.6.7)_2(3.4^2.5^2.7)(4.10^2)(4^3.6^2.8)$. It is worth noting that this net seems quite like a zeolite and also has mutidimensional channels. Actually, from the view of pure topology, it can be further simplified into zeolite topology, by incorporating the pairwise 3-connected nodes into a new 4-connected node (T1; Figure 7b, Figure S4, Supporting Information). The long Schläfli symbol for the newly created T1 node is $4.4.8.8.9_2.10_2$, and its amount is half of the other 4-connected nodes. Therefore, the 5-nodal zeolite net has a short symbol of $(3.4^2.5.6.7)_4(3.4^2.5^2.7)_2(4^2.8^2.9.10)(4^3.6^2.8)_2$ (Figure 7c).

In summary, we have synthesized five hybrid inorganic−organic materials by the assembly of $Pb^{2+}$ ions and different aromatic carboxylic acids. The lead cations in these compounds are in either hemi- or holodirected geometry with the coordination numbers in the range of 6−9, and the aromatic carboxylic ligands represent various coordination modes (Figure S1, Supporting Information, Table 3). Except for the 2D layered **IV**, the other four complexes are all 3D structures. Interestingly, they

**Table 2.** Schläfli Symbols for the Nodes in the Topological Nets of Complex **V**.

| net | symbols for nodes | | | | | symbols for nets |
|---|---|---|---|---|---|---|
| (3,4)-connected net | Pb1<br>3.4.4.7.5.6 | Pb2<br>4.4.4.8.6.6 | Pb3<br>4.10.10 | Pb4<br>3.7.4.4.5.5 | Pb5<br>3.4.4.7.5.6 | $(3.4^2.5.6.7)_2(3.4^2.5^2.7)\ (4.10^2)(4^3.6^2.8)$ |
| Zeolite net | Pb1<br>3.4.4.7.5.6 | Pb2<br>4.4.4.8.6.6 | T1<br>$4.4.8.8.9_2.10_2$ | Pb4<br>3.7.4.4.5.5 | Pb5<br>3.4.4.7.5.6 | $(3.4^2.5.6.7)_4(3.4^2.5^2.7)_2\ (4^2.8^2.9.10)(4^3.6^2.8)_2$ |

**Table 3.** Coordination Modes of the Aromatic Carboxylic Ligands in Complexes **I**−**V**

| complex | coordination modes |
|---|---|
| **I** | $\mu_6$-($\eta_2$-O,O′),($\eta_2$-O″,O‴),O′,O″,O⁗,O⁗′ |
| **II** | $\mu_7$-($\eta_2$-O,O′),($\eta_2$-O″,O‴),($\eta_2$-O⁗,O⁗′),O″,O‴,O⁗,O⁗′ |
| **III** | $\mu_6$-($\eta_2$-O,O′),O,O″,O‴,O⁗,O⁗′ |
| **IV** | $\mu_5$-($\eta_2$-O,O′),($\eta_2$-O′,O″),O,O‴,O‴′ ; $\mu_6$-($\eta_2$-O,O′),($\eta_2$-O′,O″),O′,O″,O‴,O‴′ |
| **V** | $\mu_3$-($\eta_2$-O,O′),O″,O‴; $\mu_5$-($\eta_2$-O,O′),O,O″,O″,O‴; $\mu_4$-O,O,O′,O′; $\mu_8$-O,O,O′,O′,O″,O″,O‴,O‴; $\mu_6$-($\eta_2$-O,O′),($\eta_2$-O″,O‴),O,O′,O″,O‴ |

**Scheme 1**

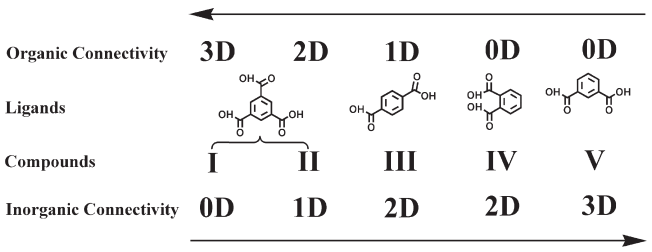


represent different inorganic Pb−O−Pb arrays: a 0D inorganic cluster for **I**, a 1D inorganic chain for **II**, a 2D inorganic layer for **III** and **IV**, and a 3D inorganic skeleton for **V** (Scheme 1). This variation might be due to the nature of different ligands. For the reason that the sum of the organic and inorganic connectivity gives the overall dimensionality of the structure, decreasing the number of bridging functionalities of ligands will be favorable for increasing inorganic connectivity. Accordingly, in this context, Pb−benzenedicarboxylates (**III**, **IV**, and **V**) possess higher inorganic connectivity than Pb−benzenetricarboxylates (**I** and **II**).

**Thermogravimetric Analysis (TGA-MS).** To study the thermal stability of complexes **I**−**V**, TGA coupled with QMS analysis was performed on polycrystalline samples under a $N_2$ atmosphere with a heating rate of 10 °C $min^{-1}$ in the temperature range 30−1000 °C (Figure S5, Supporting Information). The phase purity of the bulk materials was confirmed by the comparison of their powder diffraction (XRD) patterns with those calculated from single-crystal X-ray diffraction studies (Figure S6, Supporting Information). For complex **I**, there is an initial weight loss of the coordinated water molecules between 125 and 225 °C. The calculated loss is 2.74%, and the observed loss is 2.63%. Then, the $\mu_3$ hydroxyl begins to be released, and the whole structure accordingly starts to collapse with a continuous weight loss until 475 °C. The residuals may be PbO, and the total weight loss is 34.06% (calcd 32.00%). The TGA curve of complex **II** also exhibits two weight losses. The first step between 150 and 220 °C corresponds to the loss of coordinated water (calcd, 3.96%; found, 4.03%). The following step until 500 °C is the release of organic ligands, with a total weight loss of 37.18% (calcd, 37.37%). Complex **III** manifests high thermal stability with its TGA curve unchanged from room temperature to 300 °C. Then, the whole structure begins to decompose due to the loss of bridging ligands. The framework of complex **IV** can even be retained up to 350 °C, indicating a higher stability. And the total weight loss from 350 to 800 °C is 37.88%, corresponding to the release of ligands (calcd, 38.36%). For complex **V**, the first weight loss of 2.69% (calcd, 2.37%) in the temperature range 200−250 °C is equivalent to the release of three water molecules. Powder XRD patterns confirm that the structure of **V** can remain stable up to 300 °C (Figure S6e, Supporting Information). Then, the whole framework begins to collapse until 475 °C, with a total weight loss of 41.31% (calcd, 41.93%). The residue is PbO according to the powder XRD result. The thermal behavior of these five complexes is further confirmed by the ion-current signals of $H_2O$ ($m/z$ 18) and $CO_2$ ($m/z$ 44) in their QMS curves.

**Photoluminescence Properties.** $Pb^{2+}$ has interesting photochemical and photophysical properties. However, compared with transition metals and lanthanide, relatively little attention has been paid to the photoluminescence research of coordination complexes of lead. In this study, the photoluminescence properties of complexes **I**−**V** have been explored in the solid state at room temperature (Figure 8). And in order to understand the nature of these emission bands, we have also examined the luminescent properties of free ligands. The free ligands display emission at 440 nm ($\lambda_{ex}$ = 325 nm) for 1,3,5-$H_3$BTC, at 385 nm ($\lambda_{ex}$ = 335 nm) for 1,4-$H_2$BTC, at 330 nm ($\lambda_{ex}$ = 310 nm) for 1,2-$H_2$BTC, and at 350 nm ($\lambda_{ex}$ = 310 nm) for 1,3-$H_2$BTC.[8a,16] These emission bands of free ligands can probably be assigned to the $\pi \rightarrow \pi^*$ transitions. For the complexes, the emission bands are 475 nm ($\lambda_{ex}$ = 325 nm) for **I**, 480 nm ($\lambda_{ex}$ = 330 nm) for **II**, 520 nm ($\lambda_{ex}$ = 310 nm) for **III**, 420 nm ($\lambda_{ex}$ = 310 nm) for **IV**, and 480 nm ($\lambda_{ex}$ = 330 nm) for **V**. In contrast with the luminescent properties of corresponding free ligands, the excitation wavelengths of complexes are basically consistent, while the emission wavelengths become longer and are also different from those of metal-centered transition involved s and p orbitals of $s^2$-metal cluster compounds.[17] Therefore, the emission bands of **I**−**V** should be attributed to ligand-to-metal charge transfer between

(16) (a) Yang, E. C.; Zhao, H. K.; Ding, B.; Wang, X. G.; Zhao, X. J. *Cryst. Growth Des.* **2007**, *7*, 2009. (b) Chen, W.; Wang, J. Y.; Chen, C.; Yue, Q.; Yuan, H. M.; Chen, J. S.; Wang, S. N. *Inorg. Chem.* **2003**, *42*, 944.

(17) (a) Deacon, G. B.; Phillips, R. J. *Coord. Chem. Rev.* **1980**, *33*, 227. (b) Ford, P. C.; Vogler, A. *Acc. Chem. Res.* **1993**, *26*, 220.

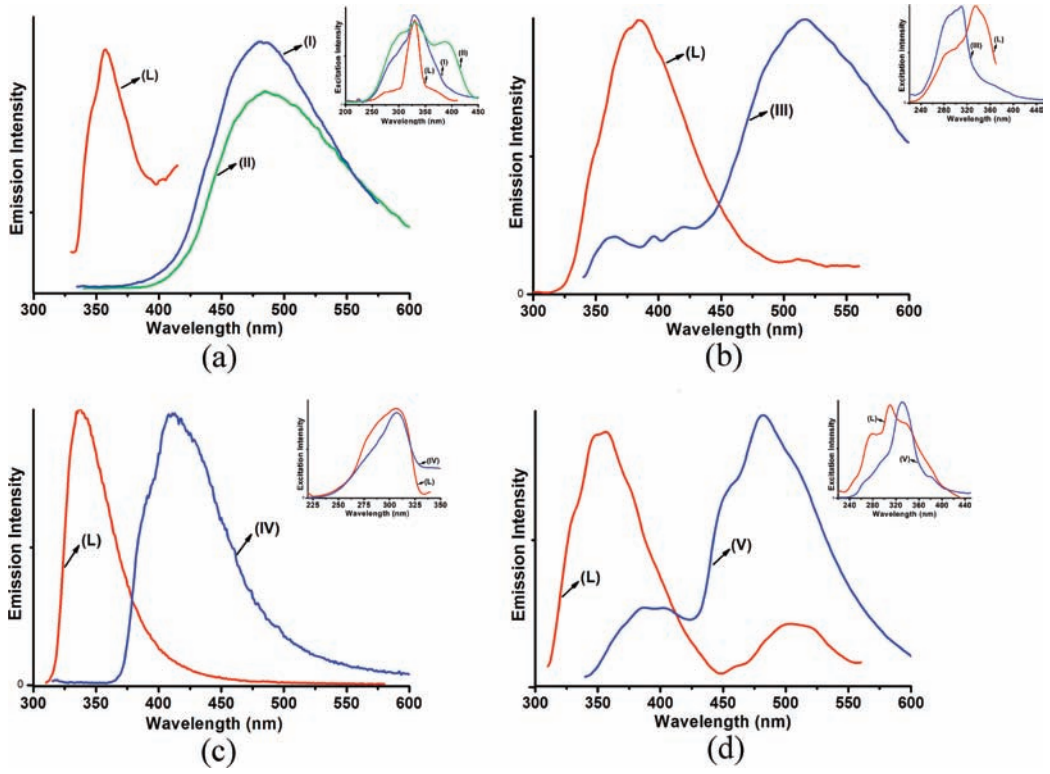


**Figure 8.** Emission and excitation spectra for 1,3,5-BTC and **I** and **II** (a), 1,4-BDC and **III** (b), 1,2-BDC and **IV** (c), and 1,3-BDC and **V** (d) in the solid state at room temperature (red for ligands, green and blue for complexes).

**Table 4.** Photoluminescence Data for Ligands and Complexes **I**−**V**

| complex | inorganic connectivity | accumulation mode | $\lambda_{ex}$ (nm) | $\lambda_{em}$ (nm) | ligand $\lambda_{ex}$ (nm) | ligand $\lambda_{em}$ (nm) | bathochromic shift of $\lambda_{em}$ (nm) |
|---|---|---|---|---|---|---|---|
| **I** | 0D | edge-sharing | 325 | 475 | 325 | 440 | 35 |
| **II** | 1D | edge-sharing | 330 | 480 | 325 | 440 | 40 |
| **III** | 2D | edge-sharing | 310 | 520 | 335 | 385 | 135 |
| **IV** | 2D | edge and corner-sharing | 310 | 420 | 310 | 330 | 90 |
| **V** | 3D | edge and corner-sharing | 330 | 480 | 310 | 350 | 130 |

delocalized $\pi$ bonds of these aromatic carboxylates groups and p orbitals of $Pb^{2+}$ centers.[18]

It should be noted that the bathochromic shift of emission bands between ligands and complexes is affected by the tightness of inorganic arrays in these complexes. As shown in Table 4, the 0D $Pb_4O_{16}$ cluster and 1D Pb−O−Pb chain give only 35 and 40 nm bathochromic shifts in **I** and **II**. When the inorganic array becomes a 2D Pb−O−Pb layer in **III** and **IV**, the bathochromic shifts increase to 135 and 90 nm, respectively. And because the accumulation mode of lead oxide polyhedra in **III** is edge-sharing, which is closer than that of the corner-sharing mode in **IV**, the bathochromic shift of **III** is much larger than that of **IV**. Although **V** has the highest inorganic connectivity of 3D, its bathochromic shift is 130 nm, near that of **III**, also owing to its loose corner-sharing accumulation mode.

## Conclusions

A series of hybrid inorganic−organic framework materials based on Pb−aromatic carboxylates have been prepared and characterized, in which the degree of inorganic connectivity has intense diversity ($I^0O^3$ to $I^1O^2$ to $I^2O^1$ to $I^2O^0$ to $I^3O^0$). Complex **I** is a three-dimensional structure with no infinite Pb−O−Pb linkages and represents the rare flu topology. Complexes **II** and **III** are also three-dimensional structures and have 1D and 2D infinite Pb−O−Pb linkages, respectively. Complex **IV** is based on a 2D inorganic Pb−O−Pb layer with organic ligands residing at its two sides. Complex **V** possesses 3D inorganic connectivity, which is first obtained in aromatic carboxylates and represents a zeolite-like topology. Compared with luminescent properties of corresponding organic ligands, under similar excitation conditions, the inorganic Pb−O−Pb linkages bring prominent bathochromic effects on the emission bands of complexes. This proves that extended inorganic hybrids can result in attractive physical properties, which are worth further investigation.

**Acknowledgment.** This work was supported by the 973 Program (2007CB815302, 2009CB939803), the Chinese Academy of Sciences (KJCX2.YW.319, KJCX2.YW.M10), and the Knowledge Innovation Program of the Chinese Academy of Sciences, Fund of Fujian Key Laboratory of Nanomaterials (2006L2005).

**Supporting Information Available:** Crystallographic data in CIF format, selected bond lengths and angles, X-ray powder diffraction patterns, TGA-MS curves for complexes **I**−**V**. These materials are available free of charge via the Internet at http://pubs.acs.org.

(18) Blasse, G.; Grabmaier, B. C. *Luminescent Materials*; Springer Verlag: Berlin, 1994.